Applied Surface Science 285P (2013) 865–873

Contents lists available at ScienceDirect

Applied Surface Science

journal homepage: www.elsevier.com/locate/apsusc

Preparation, characterization and adsorption properties of chitosan modified magnetic graphitized multi-walled carbon nanotubes for highly effective removal of a carcinogenic dye from aqueous solution

HuaYue Zhu[a,b], YongQian Fu[a], Ru Jiang[a,b,*], Jun Yao[a], Li Liu[b], YanWen Chen[a], Ling Xiao[b], GuangMing Zeng[c,**]

[a] Laboratory of Bioresource Utilization and Pollution Control, College of Life Science, Taizhou University, Taizhou 318000, Zhejiang, PR China
[b] Hubei Biomass-Resource Chemistry and Environmental Biotechnology Key Laboratory, Wuhan University, Wuhan 430072, Hubei, PR China
[c] Key Laboratory of Environmental Biology and Pollution Control, Hunan University, Ministry of Education, Changsha 410082, Hunan, PR China

ARTICLE INFO

Article history:
Received 24 June 2013
Received in revised form 31 August 2013
Accepted 1 September 2013
Available online 8 September 2013

Keywords:
Adsorption
Graphitized multi-walled carbon nanotubes
Magnetic separation
Dye
Chitosan

ABSTRACT

Novel chitosan-modified magnetic graphitized multi-walled carbon nanotubes (CS-m-GMCNTs) were synthesized via a suspension cross-linking method. Composition, morphology and magnetic properties of as-prepared CS-m-GMCNTs were characterized by XRD, SEM-EDS, BET and VSM. The large saturation magnetization (12.27 emu g^{-1}) allows fast separation of CS-m-GMCNTs from treated aqueous solution. The adsorption of congo red (CR) on CS-m-GMCNTs was strongly dependent on pH, temperature of the aqueous phase and adsorbent dosage. Up to 100 and 94.58% color removal could be achieved in 100 min contact time with 10 and 50 mg L^{-1} of initial concentrations, respectively. The adsorption capacity of CR onto CS-m-GMCNTs could reach 262.9 mg g^{-1}. The pseudo-second-order kinetic model with high correlation coefficients ($R^2 > 0.999$) was suitable to describe the process of CR adsorption onto CS-m-GMCNTs. The Langmuir model fitted the adsorption isotherm data better than the Freundlich model. Values of thermodynamic parameters (ΔG°, ΔH° and ΔS°) indicated that the adsorption process was strongly dependent on temperature of the aqueous phase, and spontaneous and endothermic process in nature. Therefore, CS-m-GMCNTs adsorbent displays main advantages of excellent dispersion, convenience separation and high adsorption capacity, which implies their potential application in the environmental cleanup.

1. Introduction

Carbon nanotubes (CNTs) have attracted special interest in interdisciplinary fields owing to their large specific surface area, highly porous and hollow structure, which has shown promising applications in many areas including environmental engineering since their discovery in 1991 by Iijima [1–4]. Recently, numerous studies have demonstrated their potential application in adsorption removal of different pollutants such as metallic ions [5,6], synthesized dye [7], and other hazardous organic compounds [8]. Generally, adsorption capacities of CNTs toward these pollutants were superior to those of activated carbon, which resulted from the stronger interactions between objective pollutants and CNTs [5]. However, some obvious obstacles of raw CNTs, such as poor dispersion in aqueous solutions, lack of surface functional groups and the difficulty in collecting them from the treated effluents greatly restricted their actual application in the removal of pollutants [9].

Recently, modification of CNTs with biopolymers has attracted significant interest due to their hydrophilicity, excel dispersion in aqueous solution and excellent adsorption properties [3,4,10–12]. It opens up new prospects for the preparation and application of novel biopolymer modified CNTs materials. Among those biopolymers used, chitosan is a kind of excellent adsorbent for the removal of dyes and metal ions in aqueous solution due to its high content of hydroxyl and amino groups in the polymer chains [13,14]. By sonication or covalent modification, chitosan and its derivatives could be grafted onto the surface of CNTs, resulting in provisionally stable suspension of CNTs in acidic or neutral aqueous solutions [4,10,15–18]. Some studies have demonstrated that the dispersion of CNTs could be dramatically improved using chitosan possibly due to a higher surface coverage of the CNTs [12,19]. Except for the excellent dispersion, chitosan/CNTs nanocomposite also possessed higher adsorption capacities for removing many kinds of organic

* Corresponding author at: No. 1139, Municipal Government Avenue, Jiaojiang District, Taizhou City, Zhejiang Province 318000, PR China. Tel.: +86 158 6763 6396; fax: +86 576 8513 7066.
** Co-corresponding author. Tel.: +86 731 8822 754; fax: +86 731 8823 701.
E-mail addresses: jiangru0576@163.com (R. Jiang), zgming@hnu.cn (G. Zeng).

0169-4332/$ – see front matter © 2013 Elsevier B.V. All rights reserved.
http://dx.doi.org/10.1016/j.apsusc.2013.09.003

and inorganic pollutants such as 4,4-dichlorobiphenyl [8], synthesized azo dye [20] and heavy metals [21]. Generally, the numerous hydroxyl and amino groups in the polymer chains of chitosan resulted in an obvious enhancement in the adsorption of pollutants on chitosan/CNTs nanocomposite. However, the difficulty in collecting these chitosan/CNTs nanocomposite from treated effluents can cause inconvenience in their practical application. Therefore, it is necessary and significant to explore novel functionalized chitosan/CNTs nanocomposite that are able to be easily separated from the treated solution except for excellent dispersion in solution and adsorption property. Recently, magnetic chitosan and magnetic carbon nanotubes for removal of pollutants from aqueous solutions have been obtained and studied since magnetic separation technique has some advantages, such as high efficiency, cost-effectiveness [5–7,22–28]. However, to the authors' knowledge, there are rarely been reported to explore the potentiality of combining these two magnetic adsorbents and using it for effective removal of a carcinogenic textile dye from aqueous environments.

Based on the above considerations, novel chitosan-modified magnetic graphitized multi-walled carbon nanotubes (CS-m-GMCNTs) were synthesized via a suspension cross-linking method and characterized by XRD, SEM-EDS, BET and VSM in this study. The obtained magnetic CS-m-GMCNTs were used as an adsorbent for effective removal of a carcinogenic textile dye, congo red (CR in chief), from aqueous solutions. The adsorption isotherm, kinetics, thermodynamics, and mechanisms involved in the adsorption process were also discussed, which would provide a theoretical foundation for further applications of system design in the sequestration or removal of hazardous pollutants.

2. Experimental

2.1. Chemicals

Graphitized multi-walled carbon nanotubes (GMCNTs in chief, purity > 99.9 wt%, diam. 15 ± 5 nm, length 10–30 μm) were purchased from Chengdu Organic Chemistry Co., Ltd., Chinese Academy of Sciences (Chengdu, China). Chitosan with 91% degree of deacetylation (DD) and 2.1×10^5 of molecular weight was purchased from Yuhuan Jinke Co., Ltd. (Taizhou, China). Congo red ($C_{32}H_{22}N_6O_6S_2Na_2$, molecular weight 696.67) used as a model carcinogenic dye was purchased from Yongjia Fine Chemical Factory (Wenzhou, China). N_2 with 99% in purity was used as protective gas from Haitian-Gas Co., Ltd. (Taizhou, China). $FeSO_4{\cdot}7H_2O$, $Fe(NO_4)_3{\cdot}9H_2O$ and other reagents of analytical grade were purchased from Shanghai Chemical Reagents Research Institute. All reagents were used without further treatment.

2.2. Preparation of Fe_3O_4 nanoparticles

Fe_3O_4 nanoparticles were prepared by co-precipitating ferric and ferrous salts in anaerobic conditions and treating under hydrothermal conditions according to the modified method [29]. Ferric and ferrous ions (molar ratio 2:1) were dissolved in deoxygenated double-distilled water at a total concentration of 0.3 M iron ions under the protection of N_2. After 30 min, the mixed solution of iron salts was added to 200 mL of chitosan-acetic acid solution (0.25 wt%) under vigorous stirring in a N_2 atmosphere. Chemical precipitation was achieved at 343 K by adding 40 mL of NH_4OH solution (29.6%, v/v) with continuously vigorous stirring. During the reaction process, the pH was maintained at about 10. The precipitates were kept at 343 K for 20 min. After the suspension was heated up to 353 K and kept for 5 h, the suspension was cooled down to room temperature and the precipitates (magnetite) were separated by magnetic decantation. Separation-redispersion cycles were carried for several time with ethanol and distilled water and then finally dried in a vacuum oven at 353 K.

2.3. Preparation of CS-m-GMCNTs

The magnetic CS-m-GMCNTs were prepared via a suspension cross-linking method. The procedure was as follows: 0.2 g chitosan was dissolved in 40 mL of acetic acid aqueous solution (2%, v/v). 0.4 g Fe_3O_4 nanoparticles and 0.4 g GMCNTs were dispersed in a solution with 80 mL paraffin and 4 mL span-80 and the mixture was mechanically stirred for 30 min. After a steady emulsion had formed, 2.0 mL of glutaraldehyde solution (25%, v/v) was added and the crosslinking reaction was allowed to proceed for 1 h at 343 K under stirring. The temperature was further increased to 353 K and the pH was adjusted to 9–10. A black product (CS-m-GMCNTs) appeared and was separated from the reaction system by a magnet and washed for three times with N,N-dimethylformamide, ethanol and distilled water, respectively. Finally, CS-m-GMCNTs were dried in an oven at 353 K under atmospheric condition.

2.4. Characterization of CS-m-GMCNTs

X-ray diffraction (XRD) measurements were performed on powdered samples in a Bruker Advance D8 X-ray diffractometer. The voltage and current used were 40 kV and 30 mA, respectively, and XRD patterns were obtained in the 2θ range of 10°–70° at 5° min^{-1} scanning speed. CS-m-GMCNTs were mounted onto stubs using a double sided adhesive tape and coated with gold. The coated samples were observed using a Hitachi SX-650 scanning electron microscope with the energy dispersive spectrometer (EDS) at the required magnification. A commercial HH-15 model vibrating sample magnetometer (VSM) (Nanjing University, China) was used at room temperature to characterize the magnetic properties of CS-m-GMCNTs. N_2 adsorption-desorption isotherms on CS-m-GMCNTs at 77 K was measured on a Micromeritics ASAP2020, from which the Brunauer–Emmett–Teller (BET) surface area and Barrett–Joyner–Halenda (BJH) pore size were calculated, respectively.

2.5. Batch adsorption studies

Batch adsorption experiments were carried out on a model KYC-1102C thermostate shaker (Ningbo, China). For a typical batch experiment, about 50 mg of CS-m-GMCNTs was incubated with 50 mL of CR solution for 3 h. At completion of predetermined time intervals, 5 mL of dispersion was drawn and CS-m-GMCNTs adsorbent was separated immediately by a magnet from treated solutions. Residual CR concentration in supernate was analyzed at $\lambda_{max} = 496.0$ nm using a Cary 50 model UV–visible spectrophotometer (Varian, USA). Adsorbed amount (q_t) of CR per unit weight of dry CS-m-GMCNTs at time t and removal efficiency (η) of CR on CS-m-GMCNTs were calculated by Eqs. (1) and (2), respectively.

$$q_t = \frac{(C_0 - C_t)V}{W} \quad (1)$$

$$\eta(\%) = \frac{C_0 - C_t}{C_0} \times 100 \quad (2)$$

where C_0 and C_t (mg L^{-1}) are the initial CR concentration and the CR concentrations at any time t (min), respectively; V (L) is the volume of the CR solution; and W (g) is the weight of CS-m-GMCNTs used.

All adsorption experiments were performed in triplicate, and the averaged values were taken and reported in this study.

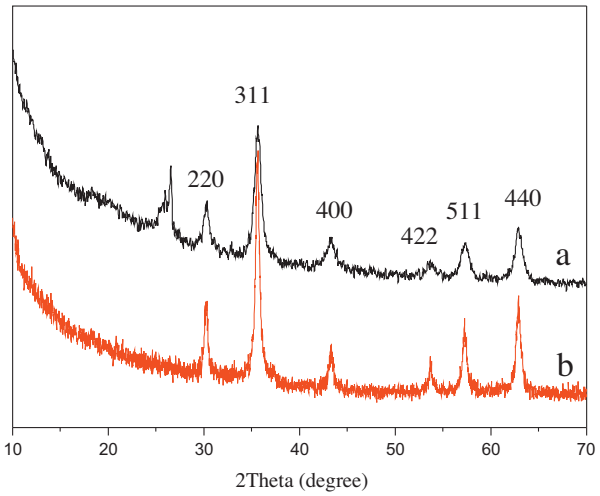

Fig. 1. XRD patterns of CS-m-GMCNTs (a) and Fe_3O_4 (b).

3. Results and discussion

3.1. Characteristics of CS-m-GMCNTs

3.1.1. X-ray diffraction (XRD)

Fig. 1 showed the XRD patterns of CS-m-GMCNTs and as-prepared Fe_3O_4 nanoparticles. The XRD patterns of CS-m-GMCNTs and pure Fe_3O_4 particles were mostly coincident. There are six characteristic peaks for Fe_3O_4 ($2\theta = 30.1^\circ$, 35.5°, 43.3°, 53.4°, 57.2°, and 62.5°), where all diffraction peaks can be well indexed to the (2 2 0), (3 1 1), (4 0 0), (4 2 2), (5 1 1), and (4 4 0) planes (JCPDS No. 19-0629), indicating that both Fe_3O_4 and CS-m-GMCNTs exhibited typical Fe_3O_4 cubic structure. The weaker diffraction lines of CS-m-GMCNTs indicate that the Fe_3O_4 particles were successfully coated by amorphous CS on the surface of GMCNTs.

3.1.2. SEM and EDS

Scanning electron microscopy (SEM) was used to study the morphology of CS-m-GMCNTs and the corresponding results are shown in Fig. 2. Fig. 2(a) showed that CS-m-GMCNTs were cylindrical in shape with an average diameter of 36 nm and tangled together, which was wider than raw GMCNTs (diam. 15 ± 5 nm). The surfaces of carbon nanotubes in CS-m-GMCNTs were rough and existed some clusters attached to them (shown in Fig. 2(b)). The phenomenon indicated that chitosan macromolecular and Fe_3O_4 have been grafted on the surface of GMCNTs by the formation of amide linkages between the reactive primary amine groups of chitosan and the carboxylic groups of GMCNTs [8,30]. In order to further confirm the composition on the surface of CS-m-GMCNTs, the energy-dispersive spectra (EDS) from different sample spots were performed. The EDS spectra of CS-m-GMCNTs and the quantitative elemental composition were shown in Fig. 2(c) and (d). Fig. 2(c) and (d) confirmed the presence of C, O and Fe in CS-m-GMCNTs. The C signal is originated from the GMCNTs and chitosan while the Fe signal came from the Fe_3O_4 nanoparticles, which confirms the existence of Fe_3O_4, consistent with the results of XRD and SEM. However, comparing EDS from different sample spots, there is a different distribution of Fe_3O_4 nanoparticles in the EDX spectrum. The quantity of Fe_3O_4 on the surface of CS-m-GMCNTs (Fig. 2(d)) was higher than that of another sample spot, which indicated that Fe_3O_4 nanoparticles were mainly formed around the GMCNTs.

3.1.3. Vibrating-sample magnetometer (VSM)

Fig. 3 showed the magnetization of Fe_3O_4 and CS-m-GMCNTs as a function of applied magnetic fields at 300 K. As can be seen in Fig. 3, the corresponding magnetization of both Fe_3O_4 and CS-m-GMCNTs increased with an increase in the magnetic fields and the saturated magnetization (σ_s) of Fe_3O_4 and CS-m-GMCNTs were 67.67 and 12.27 emu g^{-1}, respectively, which was higher than those of other magnetic CNTs reported in previous literatures [26,31]. Both Fe_3O_4 and CS-m-GMCNTs showed the characteristics of super paramagnetism since they exhibited low remanence and coercivity, which indicated that the diameter of Fe_3O_4 in both Fe_3O_4 and CS-m-GMCNTs was less than 30 nm [32].

Generally, GMCNTs are very difficult to disperse and form a stable suspension in aqueous solution because of their strong hydrophobic graphite structures (Fig. 4(a)). With the introduction of chitosan, CS-m-GMCNTs were successfully dispersed and formed a very stable suspension in aqueous solution, as shown in Fig. 4(b). CS-m-GMCNTs had a strong magnetism according to the results of VSM measurement, which made them convenient to be separated and reclaimed from treated solution after adsorption. The

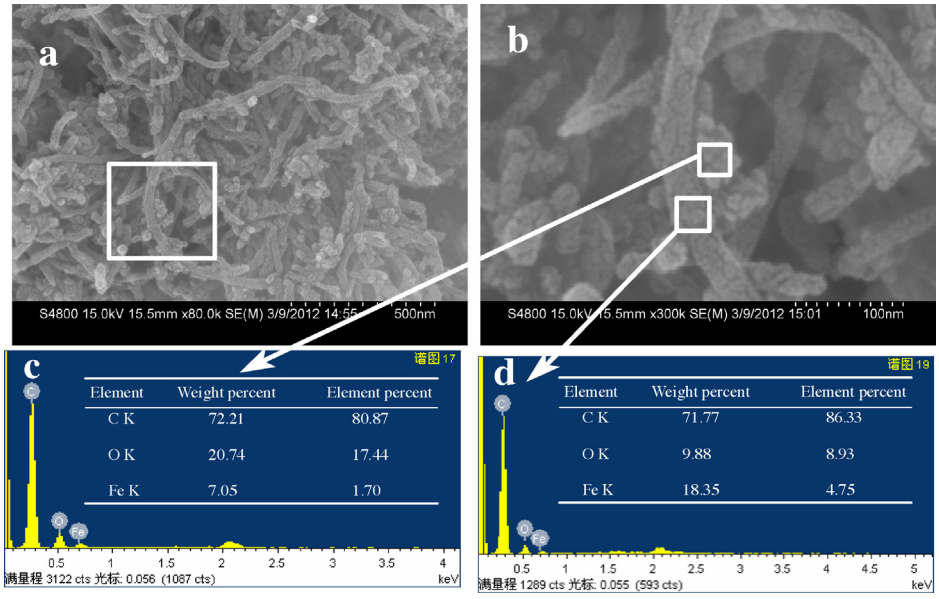

Fig. 2. SEM images (a and b) and energy-dispersive spectra (EDS) (c and d) of CS-m-GMCNTs.

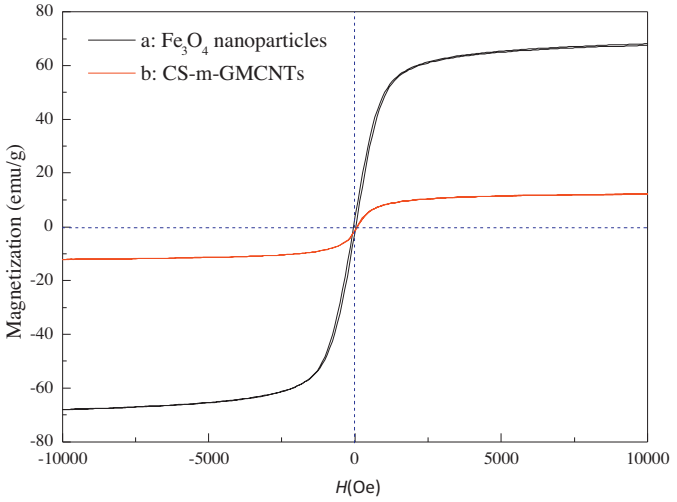

Fig. 3. Magnetic hysteresis curves of Fe_3O_4 (a) and CS-m-GMCNTs (b).

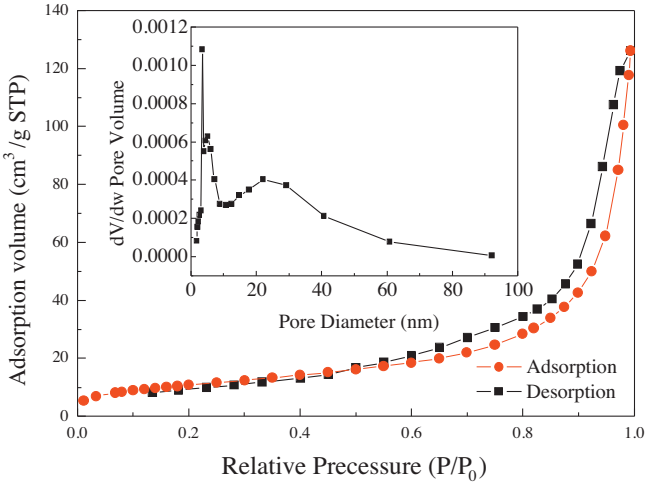

Fig. 5. BET adsorption–desorption isotherms and pore volume distribution (inset) of CS-m-GMCNTs.

CS-m-GMCNTs showed a tendency to be attracted by a permanent magnet and the CR solution turned transparent and colorless after the recycling of CS-m-GMCNTs from treated solution when a permanent magnet was placed nearby (Fig. 4(c) and (d)). Therefore, the prepared CS-m-GMCNTs adsorbent displayed the main advantages of the convenient recycling from aqueous solution and high adsorption capacity, which implied their potential application for effective removal of dye molecules and other pollutants from aqueous solution.

3.1.4. Brunauer–Emmett–Teller (BET) surface area

The BET surface area and pore structure of the as-prepared CS-m-GMCNTs have been investigated using N_2 adsorption–desorption measurements and the corresponding result is displayed in Fig. 5. The BET surface area of CS-m-GMCNTs was obtained as 39.20 $m^2\,g^{-1}$ and the total pore volume (V_P) was obtained as 0.129 $cm^3\,g^{-1}$. A great specific surface area (39.20 $m^2\,g^{-1}$) of CS-m-GMCNTs can supply more surface active sites, leading to an enhancement of adsorption performance. It is suggested that the pore structure of the adsorbent materials used consists of macropores, mesopores and micropores. Pore volume distribution of CS-m-GMCNTs was presented in Fig. 5(inset). Two major pore widths (3.4 and 22.0 nm) were detected, which indicated that CS-m-GMCNTs have a mesoporous structure and makes it easy for CR to penetrate into the mesopores of CS-m-GMCNTs.

3.2. Effect of initial CR concentration on adsorption

The initial adsorbate concentration plays an important role in the adsorption capacity of dye on adsorbent. Fig. 6 shows the effect of different initial CR concentration on color removal and adsorption capacity (q_t) of CR onto CS-m-GMCNTs. After 20 min, decolorization efficiency of CR was 97.37%, 81.47%, 72.40%, 63.65% and 54.99% when the initial concentration was 10 mg L^{-1}, 20 mg L^{-1}, 30 mg L^{-1}, 40 mg L^{-1} and 60 mg L^{-1}, respectively. However, after 120 min, the corresponding decolorization efficiency reached to 100%, 99.28%, 99.14%, 96.97% and 94.58%, respectively. The results indicated that CS-m-GMCNTs possessed excellent adsorption property for effectively removing CR azo dye from aqueous solution. As seen in Fig. 6(b), q_t value increased evidently from 9.82 mg g^{-1} to 58.32 mg g^{-1} with the increase in initial concentration from 10 mg L^{-1} to 60 mg L^{-1}. The result that adsorption capacity of CR increased with the increasing of initial CR concentration might be attributed to an increase in the driving force of a concentration gradient with the increase in the initial concentration. For CS-m-GMCNTs, some possible interactions including electrostatic interactions, hydrogen bonds, π–π bonds, covalent and hydrophobic effect are responsible for the adsorption of organic chemicals on the surface of carbon nano-sized particles.

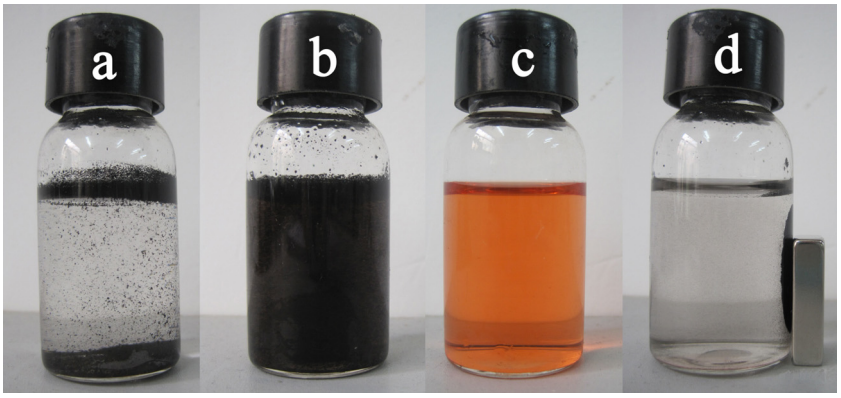

Fig. 4. Optical photographs: GMCNTs existed in aqueous solution (a), CS-m-GMCNTs dispersed in aqueous solution (b), the CR solution (c), and separation of CS-m-GMCNTs from treated CR solution by a magnet (d).

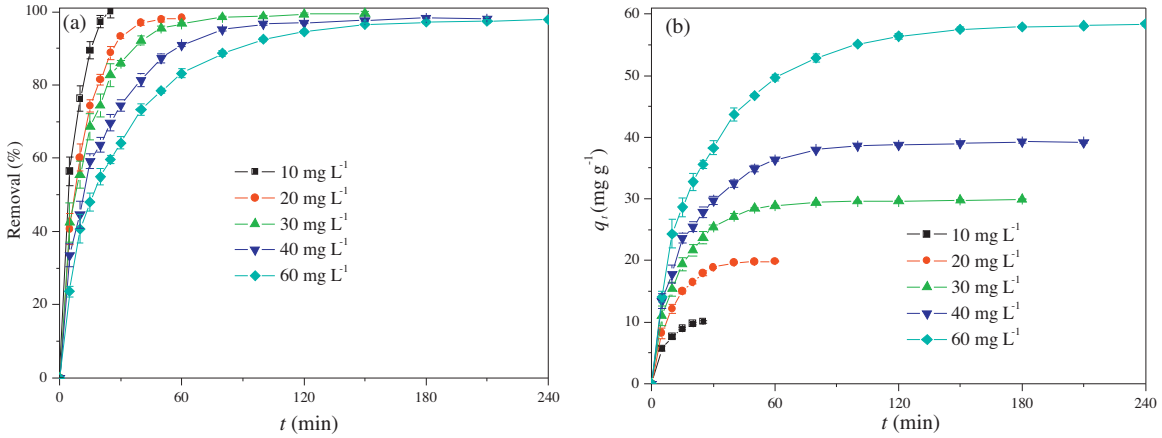

Fig. 6. Effect of initial CR concentration on the adsorption of CR by CS-m-GMCNTs (conditions: 10–60 mg L^{-1}, pH 6, 150 rpm, and 298 K).

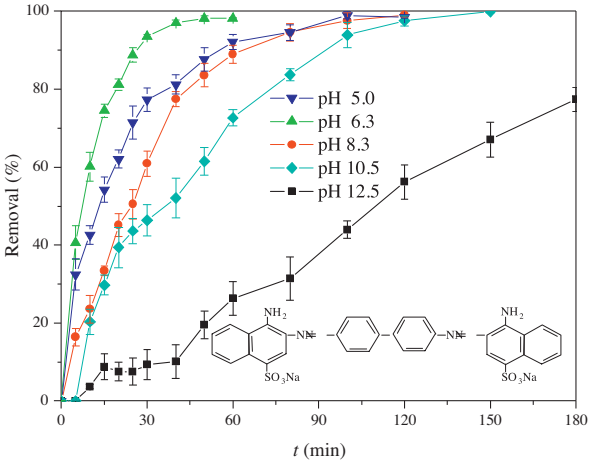

Fig. 7. Effect of pH on the adsorption of CR by CS-m-GMCNTs at 298 K and the initial dye concentration of 60 mg L^{-1}. Inset: the chemical structure of CR.

3.3. Effect of pH on adsorption

The pH may be one of the most important parameters governing adsorption of pollutants on adsorbents [33]. The effect of pH on the adsorption of CR on CS-m-GMCNTs is illustrated in Fig. 7. As shown in Fig. 7, the adsorption of CR on CS-m-GMCNTs was strongly dependent on pH. Clearly, maximum adsorption CR on CS-m-GMCNTs occurs at pH 6.3. This phenomenon could be attributed to the increased electrostatic attractions between the negatively charged dye anions and the positively charged adsorption sites of CS-m-GMCNTs at lower pH values. Two sulfonate groups of CR (shown in Fig. 7(inset)) are easily dissociated and have negative charges in the aquatic solution. Amine groups (—NH_2) that existed in chitosan molecules on the surface of CS-m-GMCNTs can be protonated as a form of —NH_3^+. In addition, an interaction between H_3O^+ ions and the cloud of π electrons of the aromatic rings of GMCNTs resulted into positive surface charge on CS-m-GMCNTs [6]. Such positively charged groups are likely to be the binding sites for adsorption of negatively charged CR from aqueous solution. At the same time, the pK_a values of amine groups in the biological molecules are known to be in the range of 8–11 [34]. On the other hand, the point of zero charge (PZC) of GMCNTs was reported to be approximately 4 [35]. Therefore, it can be postulated that with the solution pH decreases, the binding sites (positively charged amine) increase, and thereby the adsorption of CR increases.

3.4. Adsorption kinetics

The kinetics of adsorption is significant from the point of view that it controls the process efficiency [36]. Therefore, in order to investigate the kinetics of adsorption of CR onto CS-m-GMCNTs, three common adsorption kinetic equations were employed to simulate the process, that is, the Lagergren-first-order equation (Eq. (3)), pseudo-second-order equation (Eq. (4)) and intraparticle diffusion model (Eq. (5)) as expressed below:

$$\log\ (q_e - q_t) = \log\ q_e - \frac{k_1 t}{2.303} \tag{3}$$

$$\frac{t}{q_t} = \frac{1}{k_2 q_e^2} + \frac{1}{q_e} t \tag{4}$$

$$q_t = k_{id} t^{1/2} + c \tag{5}$$

where q_e and q_t are the amount of CR adsorbed (mg g^{-1}) on the adsorbents at the equilibrium and at time t, respectively; k_1 is the Lagergren-first-order rate constant of adsorption (min^{-1}). Values of k_1 is calculated from the plots of log($q_e - q_t$) versus t for different concentrations of the CR dye. k_2 is the rate constant of pseudo-second-order adsorption (g mg^{-1} min^{-1}). Values of k_2 are obtained from plotting (t/q_t) versus t. k_{id} is the intraparticle diffusion rate constant, which can be evaluated from the slope of the linear plot of q_t versus $t^{1/2}$. c is the intercept (mg g^{-1}).

Table 1
Kinetic parameters of CR adsorption onto CS-m-GMCNTs for different initial dye concentrations.

C_0 (mg L^{-1})	$q_{e,exp}$ (mg g^{-1})	Lagergren-first-order kinetic model			Pseudo second-order kinetic model		
		$q_{e,cal}$ (mg g^{-1})	k_1 (min^{-1})	R^2	$q_{e,cal}$ (mg g^{-1})	$10^3 \times k_2$ (g mg^{-1} min^{-1})	R^2
60	58.66	44.36	0.026	0.985	58.93	1.05	0.999
40	39.27	27.44	0.034	0.981	39.95	2.25	0.999
30	29.81	16.19	0.036	0.946	30.02	4.18	0.999
20	21.01	13.98	0.050	0.918	21.82	6.02	0.998
10	10.36	11.02	0.170	0.979	10.49	18.36	0.999

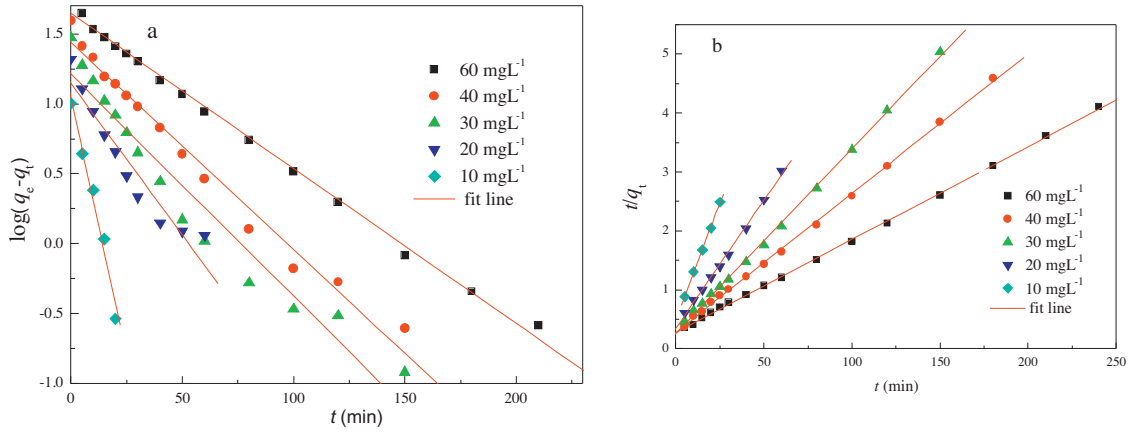

Fig. 8. First-order kinetic plots (a) and second-order kinetic plots (b) for the adsorption of CR on CS-m-GMCNTs.

Obviously, the theoretical $q_{e,cal}$ values calculated from the Lagergren-first-order kinetic model gave significantly different values compared to corresponding experimental values ($q_{e,exp}$), and the correlation coefficients ($R^2 < 0.985$) were also found to be lower (Fig. 8(a) and Table 1). These results indicated that the Lagergren-first-order kinetic model might not be sufficient to describe the adsorption process of CR on CS-m-GMCNTs. Whereas the pseudo-second-order equation showed well fit to the experimental data with higher squared correlation coefficients ($R^2 > 0.998$) (Fig. 8(b) and Table 1). The pseudo-second-order model is based on the assumption that the rate-determining step may be a chemical adsorption involving valence forces through sharing or exchange of electrons between adsorbent and adsorbate [36]. Values of k_2 decreased from 1.84×10^{-2} to 1.05×10^{-3} ($g\,mg^{-1}\,min^{-1}$) with the increase in CR solution from 10 mg L^{-1} to 60 mg L^{-1}. This result is further proven that adsorption of CR onto CS-m-GMCNTs increased with the increasing of initial CR concentration resulting from an increase in the driving force of a concentration gradient.

In order to investigate diffusion mechanism during adsorption of CR solution onto CS-m-GMCNTs, the intraparticle diffusion model (Eq. (6)) has also been studied. Generally, the interpretation of overall adsorption behavior in terms of the true diffusivity and equilibrium properties is not always straightforward. However, an apparent diffusion coefficient can be derived by fitting the adsorption experimental data obtained from the slope of the linear plot of q_t versus $t^{1/2}$. The plots of q_t versus $t^{1/2}$ for CR adsorption on CS-m-GMCNTs at different initial concentrations are shown in Fig. 9. The intraparticle diffusion constants (k_{id1}, k_{id2}) and the correlation coefficient (R^2) are shown in Table 2. According to Fig. 9, the adsorption of CR onto CS-m-GMCNTs went through three consecutive stages, which is typical adsorption onto mesoporous materials. It was in agreement with the above-mentioned discussion on the BET analysis. Generally, first stage is attributed to the external surface adsorption correlated to the boundary layer diffusion, which is assumed to occur rapidly and does not form a rate-limiting stage in the adsorption of organic pollutant on activated carbons. From Table 2, it can be seen that the order of adsorption rate in the first

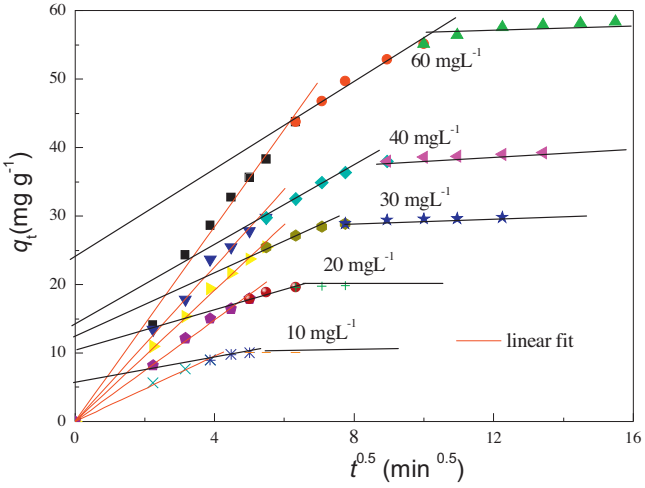

Fig. 9. Intraparticle diffusion model for the CR adsorption on CS-m-GMCNTs.

stage (k_{id1}) was higher than that in the second stage (k_{id2}) for CR adsorption on CS-m-GMCNTs. The second stage attributed to intraparticle diffusion is slower. However, values of corresponding k_{id2} increased from 0.97 to 3.08 mg g^{-1} $min^{-1/2}$ with the increase in CR solution from 10 mg L^{-1} to 60 mg L^{-1}. It is proposed that the main resistance to mass transfer occurs solely in the second stage, during the movement or diffusion of the carcinogenic dye in the internal mesoporous structure of the CS-m-GMCNTs. In addition, linear dependence for the second stage did not pass through zero, which indicated that intra-particle diffusion is involved in the adsorption process, but is not the only rate controlling step. The third stage refers to final equilibrium stage.

3.5. Adsorption isotherm

The equilibrium adsorption isotherm is fundamental in describing the interactive behavior between solutes and adsorbent, and is

Table 2
Change of slopes (k_{id}) from intraparticle diffusion model obtained for CR adsorption on CS-m- GMCNTs at different initial CR concentrations.

C_0 (mg L^{-1})	The first stage		The second stage		
	k_{id1} (mg g^{-1} $min^{-1/2}$)	R^2	k_{id2} (mg g^{-1} $min^{-1/2}$)	c (mg g^{-1})	R^2
60	7.11	0.993	3.08	24.92	0.990
40	5.65	0.993	2.40	17.21	0.989
30	4.79	0.997	1.55	17.15	0.981
20	3.71	0.996	1.21	12.03	0.976
10	2.39	0.996	0.97	5.28	0.975

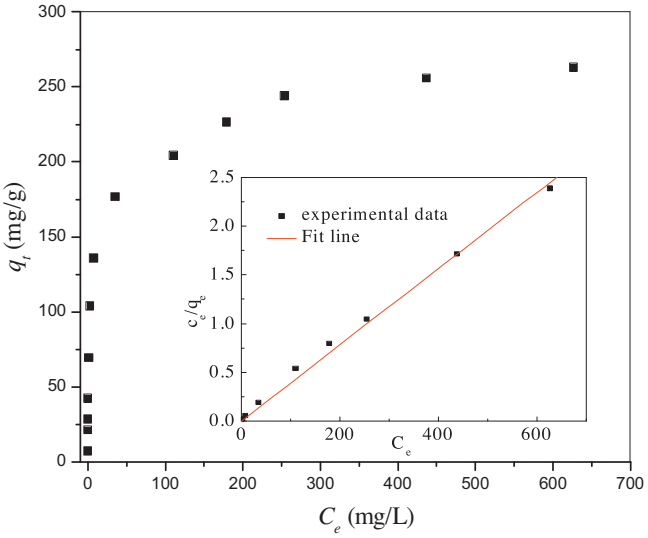

Fig. 10. Equilibrium isotherms for the adsorption of CR on CS-m-GMCNTs at 298 K. The insets illustrate the linear dependence of C_e/q_e on C_e.

important in the design of an adsorption system [37]. Adsorption experiments were conducted at 298 K to investigate the adsorption isotherm. In this work, equilibrium data for CR adsorption on CS-m-GMCNTs were modeled using the Langmuir equation (Eq. (6)) [38] and the Freundlich equation (Eq. (7)) [39]:

$$\frac{C_e}{q_e} = \frac{C_e}{q_m} + \frac{1}{K_L q_m} \tag{6}$$

$$\log\ q_e = \log K_F + \frac{1}{n} \log\ C_e \tag{7}$$

where q_m is the maximum amount of adsorption which complete monolayer coverage on the adsorbent surface (mg g^{-1}), and K_L is the Langmuir binding constant, which is related to the energy of adsorption (L mg^{-1}). C_e is the concentration of the dye solution at adsorption equilibrium (mg L^{-1}), K_F [mg g^{-1} (L g^{-1})$^{-1/n}$] and n are the Freundlich constants related to the adsorption capacity and intensity, respectively.

The results drawn from Fig. 10 and Table 3 indicated that the Langmuir model had a perfect application for CR adsorption on CS-m-GMCNTs with a regression coefficient (R^2) of 0.996 while the correlation coefficients (R^2) of Freundlich models was 0.857. In addition, the q_m value for the adsorption of CR by CS-m-GMCNTs was 261.8 mg g^{-1}, which agreed well with the experimental value $q_{e,\mathrm{exp}}$ (263.3 mg g^{-1}). Obviously, the Langmuir isotherm, compared with the Freundlich isotherm, was more suitable to describe the adsorption of CR on CS-m-GMCNTs. In other words, this adsorption process acted as monolayer adsorption on the surface of CS-m-GMCNTs under the applied experimental condition.

Further, a dimensionless constant, separation factor or "Langmuir parameter" (R_L), obtained from the Langmuir adsorption isotherm model is used to predict the favorability of the adsorption process. The R_L is equal to the ratio of the unused adsorbent capacity to the maximum adsorbent capacity and thus it can be measurement of the adsorbent capacity used and the affinity between the adsorbate and adsorbent. R_L value was calculated by the following equation (Eq. (8)):

$$R_L = \frac{1}{1 + K_L C_0} \tag{8}$$

where K_L and C_0 are Langmuir constant and initial concentration of CR, respectively.

In general, R_L classified as $R_L > 1$, $R_L = 1$, $0 < R_L < 1$ and $R_L = 0$ indicates that the type of adsorption isotherm is unfavorable, linear, favorable and irreversible, respectively. For 10–1000 mg L^{-1} of the initial CR concentrations, R_L values obtained were in the range of 0.549–0.012, suggesting that the adsorption of CR on CS-m-GMCNTs is a favorable process. In addition, the value of R_L decreased from 0.549 to 0.012 with the increase of initial CR concentration from 10 mg L^{-1} to 1000 mg L^{-1}, which could be attributed to a corresponding increase in the driving force of the concentration gradient with the increase in the initial CR concentration.

3.6. Thermodynamic parameters

The thermodynamic parameters, change in standard Gibb's free energy (ΔG°), enthalpy (ΔH°) and entropy (ΔS°) for the adsorption, were also deduced from the Langmuir adsorption data using the following equations:

$$\Delta G^\circ = -RT\ \ln K_b \tag{9}$$

$$\ln\ K_L = -\frac{\Delta H^\circ}{RT} + \frac{\Delta S^\circ}{R} \tag{10}$$

where ΔG° (kJ mol^{-1}), ΔH° (kJ mol^{-1}) and ΔS° (J mol^{-1} K^{-1}) are changes of free energy, enthalpy and entropy, respectively; R is the universal gas constant (8.314 J mol^{-1} K^{-1}) and T is the absolute temperature (K); K_b is ratio of concentration of CR on adsorbent at equilibrium (q_e) to the remaining concentration of the dye in solution at equilibrium (C_e).

Adsorption experiments were conducted at 298, 311 and 328 K to calculate thermodynamic parameters of CR on CS-m-GMCNTs. The plot of $\ln K_b$ as a function of $1/T$ yielded a straight line from which ΔH° and ΔS° were calculated from the slope and intercept, respectively. Obtained thermodynamic parameters, changes of standard Gibb's free energy (ΔG°), standard enthalpy of the process (ΔH°) and standard entropy (ΔS°) are presented in Table 4. The ΔG° values during the adsorption process were negative for

Table 3
Langmuir and Freundlish isotherm constants for the adsorption of CS-m-GMCNTs.

Langmuir isotherm constants				Freundlich isotherm constants		
$q_{e,\mathrm{exp}}$ (mg g^{-1})	$q_{m,\mathrm{cal}}$ (mg g^{-1})	K_L (L mg^{-1})	R^2	K_F (mg$^{1-(1/n)}$ L$^{1/n}$ g^{-1})	n	R^2
263.3	261.8	0.08204	0.996	3.87	3.22	0.857

Table 4
Thermodynamic parameters for CR adsorption over CS-m-GMCNTs.

Initial CR concentration (mg L^{-1})	ΔS° (J mol^{-1} K^{-1})	ΔH° (kJ mol^{-1})	ΔG° (kJ mol^{-1})		
			298 K	311 K	328 K
200	−90.11	−66.54	−8.02	−7.16	−6.88

CR at all three temperatures thereby implying that the adsorption of CR by CS-m-GMCNTs was spontaneous and thermodynamically favorable. When the temperature decreases from 328 K to 298 K, the magnitude of free energy change shifts to high negative value (from −6.88 to −8.02 kJ mol^{-1}) suggested that the adsorption was more spontaneous at low temperature. The exothermic nature of the process was once again confirmed due to negative values of enthalpy change (ΔH°), which was supported by the observation that adsorption of CR onto CS-m-GMCNTs decreased with increase in temperature. The ΔH° value (−66.54 kJ mol^{-1}) were higher than 40 kJ mol^{-1} thereby implying that the adsorption of CR onto CS-m-GMCNTs is predominantly a chemisorption process. Generally, the change of free energy for physisorption is between 0 and 20 kJ mol^{-1}, but chemisorption is a range of −63 to −84 kJ mol^{-1} [40]. Previous study also indicated that the π–π stacking is the main driving force responsible for the dye–GMCNTs interactions [34].

3.7. Comparison with other adsorbents

The maximum capacity (q_m) of CR on CS-m-GMCNTs was compared with those reported in the previous literature. The q_m value for CR adsorption on chitosan hydrobeads [41], chitosan [42], N,O-carboxymethyl-chitosan/montmorillonite nanocomposite [43], bentonite [44], mesoporous activated carbons [45] and waste red mud [46] was 92.59 mg g^{-1}, 81.23 mg g^{-1}, 74.24 mg g^{-1}, 158.7 mg g^{-1}, 52 mg g^{-1} and 4.05 mg g^{-1}, respectively. The q_m value (263.3 mg g^{-1}) for the adsorption of CR on CS-m-GMCNTs was 1.84, 2.24, 2.55, 0.66, 4.06 and 64.01 times than the corresponding q_m values of the above adsorbents, respectively. Therefore, it can be concluded that CS-m-GMCNTs shows the comparable adsorption capacity, revealing that CS-m-GMCNTs is suitable for the removal of CR from aqueous solutions.

4. Conclusion

Except for excellent dispersion, the as-prepared CS-m-GMCNTs possessed excellent adsorption properties for effective removing of a carcinogenic textile dye, congo red and excellent magnetic separation. The pseudo-second-order kinetic model with high correlation coefficients ($R^2 > 0.998$) was suitable to describe the kinetic process of CR adsorption onto CS-m-GMCNTs. Up to 100 and 94.58% color removal could be achieved in 100 min contact time from aqueous solutions with initial concentrations 10 and 60 mg L^{-1}. Magnetic measurement revealed that the saturated magnetization of CS-m-GMCNTs could reach 12.27 emu g^{-1}. The adsorption capacity of CR onto CS-m-GMCNTs could reach 263.3 mg g^{-1}. The Langmuir model fitted the adsorption isotherm data better than the Freundlich model. The values of thermodynamic parameters (ΔG°, ΔH° and ΔS°) indicated that the adsorption process was strongly dependent on temperature of the aqueous phase, and spontaneous and exothermic process. Therefore, the prepared CS-m-GMCNTs adsorbent displayed the main advantages of excellent dispersion in aqueous solution, separation convenience and high adsorption capacity, which implied their application potentials for effective removal of other carcinogenic and hazardous pollutants from aqueous solution.

Acknowledgements

Authors acknowledge the financial support from the Natural Science Foundation of China (Grant Nos. 51208331 and 21007044), the Scientific and Technological Development Project of Taizhou City in China (Grant No. 121KY05) and the Open Project form Hubei Biomass-Resource Chemistry and Environmental Biotechnology Key Laboratory of Wuhan University (Grant No. HBRCEBL2012-2013001).

References

[1] S. Iijima, Helical microtubes of graphitic carbon, Nature 354 (1991) 56–58.
[2] M.F.L. De Volder, S.H. Tawfick, R.H. Baughman, A.J. Hart, Carbon nanotubes: present and future commercial applications, Science 339 (2013) 535–539.
[3] P.R. Chang, P. Zheng, B. Liu, D.P. Anderson, J. Yu, X. Ma, Characterization of magnetic soluble starch-functionalized carbon nanotubes and its application for the adsorption of the dyes, J. Hazard. Mater. 186 (2011) 2144–2150.
[4] C. Li, K. Yang, Y. Zhang, H. Tang, F. Yan, L. Tan, Q. Xie, S. Yao, Highly biocompatible multi-walled carbon nanotube–chitosan nanoparticle hybrids as protein carriers, Acta Biomater. 7 (2011) 3070–3077.
[5] C. Chen, J. Hu, D. Shao, J. Li, X. Wang, Adsorption behavior of multiwall carbon nanotube/iron oxide magnetic composites for Ni(II) and Sr(II), J. Hazard. Mater. 164 (2009) 923–928.
[6] X. Peng, Z. Luan, Z. Di, Z. Zhang, C. Zhu, Carbon nanotubes-iron oxides magnetic composites as adsorbent for removal of Pb(II) and Cu(II) from water, Carbon 43 (2005) 855–894.
[7] J.L. Gong, B. Wang, G.M. Zeng, C.P. Yang, C.G. Niu, Q.Y. Niu, W.J. Zhou, Y. Liang, Removal of cationic dyes from aqueous solution using magnetic multi-wall carbon nanotube nanocomposite as adsorbent, J. Hazard. Mater. 164 (2009) 1517–1522.
[8] D.D. Shao, J. Hu, X.K. Wang, M. Nagatsub, Plasma induced grafting multiwall carbon nanotubes with chitosan for 4,4′-dichlorobiphenyl removal from aqueous solution, Chem. Eng. J. 170 (2011) 498–504.
[9] J. Fan, Z. Shi, Y. Ge, Y. Wang, J. Wang, J. Yin, Mechanical reinforcement of chitosan using unzipped multiwalled carbon nanotube oxides, Polymer 53 (2012) 657–664.
[10] C.K. Najeeb, J. Chang, J.H. Lee, M. Lee, J.H. Kim, Preparation of semiconductor-enriched single-walled carbon nanotube dispersion using a neutral pH water soluble chitosan derivative, J. Colloid Interface Sci. 354 (2011) 461–466.
[11] M. Fagnoni, A. Profumo, D. Merli, D. Dondi, P. Mustarelli, E. Quartarone, Water miscible liquid multiwalled carbon nanotubes, Adv. Mater. 21 (2009) 1761–1765.
[12] T. Rungrotmongkol, U. Arsawang, C. Iamsamai, A. Vongachariya, S.T. Dubas, U. Ruktanonchai, A. Soottitantawat, S. Hannongbua, Increased dispersion and solubility of carbon nanotubes noncovalently modified by the polysaccharide biopolymer, chitosan: MD simulations, Chem. Phys. Lett. 507 (2011) 134–137.
[13] H. Momenzadeh, A.R. Tehrani-Bagha, A. Khosravi, K. Gharanjig, K. Holmberg, Reactive dye removal from wastewater using a chitosan nanodispersion, Desalination 271 (2011) 225–230.
[14] M.R. Gandhi, G.N. Kousalya, N. Viswanathan, S. Meenakshia, Sorption behaviour of copper on chemically modified chitosan beads from aqueous solution, Carbohydr. Polym. 83 (2011) 1082–1087.
[15] T.X. Phuoc, M. Massoudi, R.H. Chen, Viscosity and thermal conductivity of nanofluids containing multi-walled carbon nanotubes stabilized by chitosan, Int. J. Therm. Sci. 50 (2011) 12–18.
[16] Z.G. Wu, W. Feng, Y.Y. Feng, Q. Liu, X.H. Xu, T. Sekino, Preparation and characterization of chitosan-grafted multiwalled carbon nanotubes and their electrochemical properties, Carbon 45 (2007) 1212–1218.
[17] Q. Yang, L. Shuai, X. Pan, Synthesis of fluorescent chitosan and its application in noncovalent functionalization of carbon nanotubes, Biomacromolecules 9 (2008) 3422–3426.
[18] L. Yang, B. Yang, D. Zeng, D. Wang, Y. Wang, L.M. Zhang, Formation and properties of a novel complex composed of an amylose-grafted chitosan derivative and single-walled carbon nanotubes, Carbohydr. Polym. 85 (2011) 845–853.
[19] C. Iamsamai, S. Hannongbua, U. Ruktanonchai, A. Soottitantawat, S.T. Dubas, The effect of the degree of deacetylation of chitosan on its dispersion of carbon nanotubes, Carbon 48 (2010) 25–30.
[20] C. Sudipta, T. Chatterjee, S.R. Lim, S.H. Woo, Effect of the addition mode of carbon nanotubes for the production of chitosan hydrogel core–shell beads on adsorption of congo red from aqueous solution, Bioresour. Technol. 102 (2011) 4402–4409.
[21] M.A. Salam, M.S.I. Makki, M.Y.A. Abdelaal, Preparation and characterization of multi-walled carbon nanotubes/chitosan nanocomposite and its application for the removal of heavy metals from aqueous solution, J. Alloys Compd. 509 (2011) 2582–2587.
[22] Y. Chen, J. Wang, Preparation and characterization of magnetic chitosan nanoparticles and its application for Cu(II) removal, Chem. Eng. J. 168 (2011) 286–292.
[23] D. Hritcu, D. Humelnicu, G. Dodi, M.I. Popa, Magnetic chitosan composite particles: evaluation of thorium and uranyl ion adsorption from aqueous solutions, Carbohydr. Polym. 87 (2012) 1185–1191.
[24] M. Monier, D.A. Abdel-Latif, Preparation of cross-linked magnetic chitosan-phenylthiourea resin for adsorption of Hg(II), Cd(II) and Zn(II) ions from aqueous solutions, J. Hazard. Mater. 209–210 (2012) 240–249.
[25] L. Zhou, C. Shang, Z. Liu, G. Huang, A.A. Adesina, Selective adsorption of uranium(VI) from aqueous solutions using the ion-imprinted magnetic chitosan resins, J. Colloid Interface Sci. 366 (2012) 165–172.
[26] S. Qu, F. Huang, S. Yu, G. Chen, J. Kong, Magnetic removal of dyes from aqueous solution using multi-walled carbon nanotubes filled with Fe_2O_3 particles, J. Hazard. Mater. 160 (2008) 643–647.

[27] H.Y. Zhu, Y.Q. Fu, R. Jiang, J. Yao, L. Xiao, G.M. Zeng, Novel magnetic chitosan/poly(vinyl alcohol) hydrogel beads: preparation, characterization and application for adsorption of dye from aqueous solution, Bioresour. Technol. 105 (2012) 24–30.
[28] H.Y. Zhu, R. Jiang, Y.-Q. Fu, J.H. Jiang, L. Xiaob, G.M. Zeng, Preparation, characterization and dye adsorption properties of γ-Fe_2O_3/SiO_2/chitosan composite, Appl. Surf. Sci. 258 (2011) 1337–1344.
[29] L. Liu, L. Xiao, H.Y. Zhu, Preparation and characterization of CS–Fe_3O_4@ZnS:Mn magnetic-fluorescent nanoparticles in aqueous media, Chem. Phys. Lett. 539–540 (2012) 112–117.
[30] Y.T. Shieh, Y.F. Yang, Significant improvements in mechanical property and water stability of chitosan by carbon nanotubes, Eur. Polym. J. 42 (2006) 3162–3170.
[31] J. Li, R. Hong, G. Luo, Y. Zheng, H. Li, D. Wei, An easy approach to encapsulating Fe_3O_4 nanoparticles in multiwalled carbon nanotubes, New Carbon Mater. 25 (2010) 192–198.
[32] Y. Wu, Y. Wang, G. Luo, Y. Dai, In situ preparation of magnetic Fe_3O_4-chitosan nanoparticles for lipase immobilization by cross-linking and oxidation in aqueous solution, Bioresour. Technol. 100 (2009) 3459–3464.
[33] Y. Ren, X. Wei, M. Zhang, Adsorption character for removal Cu(II) by magnetic Cu(II) ion imprinted composite adsorbent, J. Hazard. Mater. 158 (2008) 14–22.
[34] S. Wang, C. Wei Ng, W. Wang, Q. Li, Z. Hao, Synergistic, competitive adsorption of organic dyes on multiwalled carbon nanotubes, Chem. Eng. J. 197 (2012) 34–40.
[35] Z. Gao, T.J. Bandosz, Z. Zhao, M. Han, J. Qiu, Investigation of factors affecting adsorption of transition metals on oxidized carbon nanotubes, J. Hazard. Mater. 167 (2009) 357–365.
[36] G. Bayramoglu, B. Altintas, M.Y. Arica, Adsorption kinetics and thermodynamic parameters of cationic dyes from aqueous solutions by using a new strong cation-exchange resin, Chem. Eng. J. 152 (2009) 339–346.
[37] M.S. Chiou, H.Y. Li, Equilibrium and kinetic modeling of adsorption of reactive dye on cross-linked chitosan beads, J. Hazard. Mater. B 93 (2002) 233–248.
[38] I. Langmuir, The constitution and fundamental properties of solids and liquids. Part I solids, J. Am. Chem. Soc. 38 (1916) 2221–2295.
[39] H. Freundlich, Über die adsorption in lösungen (adsorption in solution), J. Phys. Chem. 57 (1906) 385–390.
[40] B. Oepen, W. Kordel, W. Klein, Sorption of nonpolar and polar compounds to soils: processes, measurements and experience with the applicability of the modified OECD Guideline 106, Chemosphere 22 (1991) 285–304.
[41] S. Chatterjee, S. Chatterjee, B.P. Chatterjee, A.K. Guha, Adsorptive removal of congo red, a carcinogenic textile dye by chitosan hydrobeads: binding mechanism, equilibrium and kinetics, Colloids. Surf. A 299 (2007) 146–152.
[42] L. Wang, A. Wang, Adsorption properties of congo red from aqueous solution onto N,O-carboxymethyl-chitosan, Bioresour. Technol. 99 (2008) 1403–1408.
[43] L. Wang, A. Wang, Adsorption behaviors of congo red on the N,O-carboxymethyl -chitosan/montmorillonite nanocomposite, Chem. Eng. J. 143 (2008) 43–50.
[44] E. Bulut, M. Özacar, İ.A. Şengil, Equilibrium and kinetic data and process design for adsorption of congo red onto bentonite, J. Hazard. Mater. 154 (2008) 613–622.
[45] E.L. Grabowska, G. Gryglewicz, Adsorption characteristics of congo red on coal-based mesoporous activated carbon, Dyes Pigm. 74 (2007) 34–40.
[46] C. Namasivayam, D.J.S.E. Arasi, Removal of congo red from wastewater by adsorption onto waste red mud, Chemosphere 34 (1997) 401–417.